

## Detecting carbon uptake and cellular allocation by individual algae in multispecies assemblages

Justin N. Murdock\*<sup>1,2</sup>

<sup>1</sup>USDA Agricultural Research Service, National Sedimentation Laboratory, Oxford, Mississippi

<sup>2</sup>Department of Biology, Tennessee Technological University, Cookeville, Tennessee

### Abstract

Algal species vary in carbon (C) need and uptake rates. Understanding differences in C uptake and cellular allocation among species from natural communities will bring new insight into many ecosystem process questions including how species changes will alter energy availability and C sequestration in aquatic ecosystems. A major limitation of current methods that measure algal C incorporation is the inability to separate the response of individual species from mixed-species assemblages. I used Fourier-transform infrared microspectroscopy to qualitatively measure inorganic <sup>13</sup>C isotope incorporation into individual algal cells in single species, two species, and natural phytoplankton assemblages. Lateral shifts in spectral peaks from <sup>13</sup>C treatments were observed in all species. Comparison of peaks associated with carbohydrates, proteins, and lipids allowed for the detection of which individuals took in C, and which macromolecules the C was used to make. For example, shifts in *Spirogyra* spectral peaks showed substantial C incorporation in carbohydrates. Further, shifts in peaks at 1160 cm<sup>-1</sup>, 1108 cm<sup>-1</sup>, 1080 cm<sup>-1</sup>, 1048 cm<sup>-1</sup>, and 1030 cm<sup>-1</sup> suggested C was being allocated into cellulose. The natural phytoplankton assemblage demonstrated how C could be tracked into co-occurring species. A diatom had large shifts in protein and carbohydrate peaks, while a green alga and euglenoid had only a few shifts in protein related peaks. Fourier-transform infrared microspectroscopy is an established, label free method for measuring the chemical composition of algal cells. However, adding a label such as <sup>13</sup>C isotope can greatly expand the technique's capabilities by qualitatively tracking C movement between inorganic and organic states within single cells.

Inorganic carbon (C) uptake by algae is a critical pathway of energy input into aquatic ecosystems, and also an important pathway for carbon dioxide (CO<sub>2</sub>) sequestration from the atmosphere. For example, algae can capture up to 99% of available dissolved CO<sub>2</sub> when grown under optimal conditions (Sayre 2010) and ocean phytoplankton have been estimated to sequester ~37 to 45 Pg of C per year (Falkowski et al. 2000; Sabine et al. 2004). Knowing which algal species within a community are most efficient in sequestering available C under varying conditions can help predict how species shifts caused by environmental changes will alter energy and nutrient input into food webs. Furthermore, knowing which cellular components algae are incorporating newly acquired C can help refine species selection for maximum C removal or biomass production in bioengineering applications. However, the importance of algal diversity and the role of individual species in assemblage level function such as nutrient cycling, primary productivity, or lipid production are not well understood beyond that of low diversity laboratory studies and cyanobacterial roles in nitrogen fixation

(e.g., Behl et al. 2011; Cardinale 2011; Corcoran and Boeing 2012).

One of the major challenges of establishing a species-specific approach to algal nutrient cycling is the technical limitation of separating cells and assessing nutrient uptake and distribution within individuals. Fourier-transform infrared (FTIR) microspectroscopy with isotope labeling can partially overcome this constraint by optically isolating a single cell from mixed-species assemblages and qualitatively measuring its relative macromolecular content. By labeling cells with <sup>13</sup>C prior to analysis, this method can determine into which macromolecules (i.e., proteins, lipids, carbohydrates) the cells allocated the newly acquired <sup>13</sup>C. FTIR microspectroscopy can further our understanding of how different algae use inorganic C at the species, individual cell, and sub-cellular levels in natural, mixed-species communities.

FTIR microspectroscopy has been used to identify the relative biochemical composition within single algal cells for over two decades (Sekkal et al. 1993; Giordano et al. 2001; Dean and Sigee 2006; Heraud et al. 2007; Murdock and Wetzel 2009). More recently, this method has been adapted to

\*Correspondence: jnmurdock@tntech.edu

**Table 1.** Macromolecular assignments of common infrared spectral peaks of carbon containing molecules in algae.

Wavenumber range (cm <sup>-1</sup> )	Assignments	Functional groups
2970–2960	$\nu_{as}$ CH <sub>3</sub>	Lipid methyl group
2930–2920	$\nu_{as}$ CH <sub>2</sub>	Lipid methylene groups
2875–2850	$\nu$ CH <sub>2</sub> , CH <sub>3</sub>	Lipid methyl and methylene groups in fatty acids
1745–1734	$\nu$ C=O	Lipid esters of membrane lipids, fatty acids
1720–1700	$\nu$ C=O	Lipid esters of carboxylic groups
1655–1638	$\nu$ C—O	Protein (Amide I). May also contain C=C stretches of olefinic and aromatic compounds
1699–1590	$\nu_{as}$ COO—	Protein carboxylic group
1545–1540	$\nu$ C—N	Protein (Amide II)
1456–1450	$\delta_{as}$ CH <sub>2</sub> , $\delta_{as}$ CH <sub>3</sub>	Lipid and protein methyl and methylene groups
1460–1392	$\nu$ C—O	Protein carboxylic group
1398–1370	$\delta$ CH <sub>3</sub> , $\delta$ CH <sub>2</sub> / $\delta$ C—O	Protein carboxylic group
1200–900	$\nu$ C—O—C	Carbohydrate, mainly polysaccharide rings
1165, 1152, 1110, 1081, 1050, 1030	$\nu$ C—O	Carbohydrate, cellulose
1150–1000	$\nu$ C—O	Carbohydrate, polysaccharides

$\nu$  = symmetric stretch,  $\nu_{as}$  = asymmetric stretch,  $\delta$  = symmetric deformation (bend),  $\delta_{as}$  = asymmetric deformation (bend). Modified from Murdoch and Wetzel 2009.

understanding algae's role in the environment by investigating how individual algae from natural communities are impacted by changing water quality (Stehfest et al. 2005; Hirschmugl et al. 2006; Dean et al. 2008), pesticides (Murdoch and Wetzel 2012), and increased CO<sub>2</sub> (Giordano and Ratti 2013). Algae allocate C into different macromolecules depending on ambient environmental conditions such as nutrient [e.g., nitrogen (N) and phosphorus (P)] availability, light, and temperature. For example, when N, P, and/or silica become limiting, algae often allocate more C into carbohydrate or lipid energy storage products, than into proteins (Beardall et al. 2001). However, there is still a gap in knowledge of how algal cells acquire and allocate nutrients relative to nutrient availability or environmental changes outside the cell. The environmental trigger that causes algae to switch which macromolecules are produced should vary among species, and each species' nutrient uptake ability and macromolecular allocation is likely unique. Given the increasing interest in understanding how algae influence C

cycling in both natural ecosystems and bioengineering applications, a better tool to link species diversity to C uptake and allocation is needed.

The work presented here expands algal FTIR analyses to qualitatively identify which cells within a natural community are incorporating inorganic C using the stable isotope <sup>13</sup>C. This method tracks which algae take up inorganic C, and into which cellular components (i.e., carbohydrates, lipids, or proteins) the newly acquired C is allocated. We used benchtop and synchrotron infrared microspectroscopy to identify <sup>13</sup>C assimilation in cells of simple species combinations and a natural phytoplankton community. The relative incorporation of labeled inorganic <sup>13</sup>C (as <sup>13</sup>CO<sub>2</sub> or H<sup>13</sup>CO<sub>3</sub>) was assessed through the lateral shifts in infrared spectra peaks of the major protein, lipid, and carbohydrate absorbance bands following isotope exposure.

### Isotope identification with FTIR

Fourier transform infrared spectra are the result of dipolar molecules absorbing discrete wavelengths of infrared light. As molecules absorb infrared light, the energy is dissipated by various but distinct vibrational motions. The particular frequency ( $\nu$ ) of infrared light absorbed is due to the bond strength (i.e., single, double, triple bonds), and the mass of each atom (which is most important for isotope tracking). Therefore, the absorbance peak locations in an infrared spectrum correspond to the relative abundance of a particular macromolecule in an algal cell (e.g., C=O ester bonds in lipids absorbs infrared light at ~1740 cm<sup>-1</sup>, Table 1). See reviews by Stuart (2005) and Movasaghi et al. (2008) for further details of FTIR spectroscopy of biological tissues. Given this weight/frequency relationship, increasing the weight of one or more atoms in a molecule will alter its vibrational frequency, and, thus, cause a downward shift in absorption peaks (i.e., peaks move to a lower wavenumber).

Stable isotopes can be used to detect nutrient incorporation into algae. When an element in a cell is replaced with an isotope of different mass, such as <sup>12</sup>C with <sup>13</sup>C, or <sup>14</sup>N with <sup>15</sup>N, a downward shift in the vibrational frequency is observed, and the peak moves to the right (Esler et al. 2000). For example, replacing <sup>14</sup>N with <sup>15</sup>N in the green alga *Cladophora glomerata* led to a 10 cm<sup>-1</sup> wavenumber shift to the right in the amide II (protein) peak following a four-day incubation in <sup>15</sup>N (Murdoch et al. 2008).

Theoretical peak shifts with the complete replacement of <sup>12</sup>C with <sup>13</sup>C can be calculated for the dominant carbon-containing macromolecules in algal FTIR spectra. These macromolecules are carbohydrates (which have several polysaccharide peaks ranging from 1200 cm<sup>-1</sup> to 900 cm<sup>-1</sup>), lipids (that have peaks mainly around 3300 cm<sup>-1</sup> for methyl groups and 1740 cm<sup>-1</sup> for esters), and proteins (that have two different amide peaks mainly at 1650 cm<sup>-1</sup> and 1550 cm<sup>-1</sup>). Potential theoretical shifts with <sup>13</sup>C replacement are presented in Supporting Information Table S1, and these

calculations provide expected targets of where to look for peak shifts. It is important to note that these values should only be used as a guide during short-term incubation studies since complete replacement of  $^{12}\text{C}$  atoms in cells is not likely to occur. Additional differences between theoretical and observed peak shifts will also likely occur because these calculations represent a diatomic (two atom) molecule, and molecular vibrations from algal cells will be collected from larger, more complex molecules, which may slightly change the response.

## Materials and procedures

### Algal isotope labeling

Three phases were used to assess the ability to detect  $^{13}\text{C}$  isotope in single cells from mixed-species assemblages; (1) a single-species incubation of the green filamentous alga *Spirogyra* sp., (2) a two-species incubation of intermixed stramenopile filaments, *Tribonema* sp., and cyanobacteria filaments, *Lyngbya* sp., and (3) an incubation of a multispecies phytoplankton assemblage from a eutrophic bayou.

### Incubator labeling experiments

Algae were labeled with  $^{13}\text{C}$  during two incubation experiments to determine which regions of the alga's infrared spectra would shift with  $^{13}\text{C}$  incorporation. Algae were collected from standing water in large plastic tubs outside of the USDA National Sedimentation Laboratory in Oxford, Mississippi. Tub water nutrient concentrations were 20  $\mu\text{g/L}$   $\text{NO}_3\text{-N}$ , 4  $\mu\text{g/L}$   $\text{NO}_2\text{-N}$ , 63  $\mu\text{g/L}$   $\text{NH}_4\text{-N}$ , and 89  $\mu\text{g/L}$   $\text{PO}_4\text{-P}$ . Alkalinity was 6 mg/L  $\text{CaCO}_3$ , and pH was 6.37.

#### Single species analysis

Two to three adjacent filaments of *Spirogyra* (typical cell size  $\sim 20 \times 100 \mu\text{m}$ ) were untangled from a *Spirogyra* dominated mat, put into four 50 mL vials and incubated in 40 mL of tub water that was filtered through a 0.7  $\mu\text{m}$  GF/F filter. Two vials were labeled with 2.5 mg  $\text{NaH}^{13}\text{CO}_3$  and two with 2.5 mg  $\text{NaH}^{12}\text{CO}_3$ . All vials had an additional 608  $\mu\text{g}$  of N and 27.6  $\mu\text{g}$  of P added to alleviate potential nutrient limitation during incubation. Tubes were sealed airtight and incubated for seven days at 23°C and 105  $\mu\text{mol quanta m}^{-2} \text{s}^{-1}$  PAR light intensity with 16: 8 h light/dark cycle. Following incubation, *Spirogyra* filaments from the two tubes of each treatment were combined, rinsed three times with buffered deionized water, and treatment samples placed on separate Mirr IR infrared reflective slides (Kevley Technologies) with forceps. Care was taken to produce a single layer of cells on slides by floating filaments in a drop of water and spreading out filaments with forceps. Slides were immediately dried at 60°C for 1 h and stored in a dark desiccator until FTIR analysis. Only filaments that dried in a single layer, and were firmly attached to the slide were measured.

#### Two species mixture

A second incubation of a mixed algal species was conducted to determine whether C uptake of two species grow-

ing physically intertwined in a mat could be isolated with this technique. Approximately 1  $\text{cm}^3$  of floating algal mat was taken from a tub adjacent to the *Spirogyra* collection tub. Adjacent sections of the mats were separated and incubated as above, except the incubation volume of filtered tub water was 45 mL, 912  $\mu\text{g}$  of N and 41.4  $\mu\text{g}$  of P were added, and constant illumination was used. Tub water nutrient concentrations were 10  $\mu\text{g/L}$   $\text{NO}_3\text{-N}$ , 5  $\mu\text{g/L}$   $\text{NO}_2\text{-N}$ , 32  $\mu\text{g/L}$   $\text{NH}_4\text{-N}$ , 13  $\mu\text{g/L}$   $\text{PO}_4\text{-P}$ . Alkalinity was 4 mg/L  $\text{CaCO}_3$ , and pH was 6.0. The mat was dominated by two loosely intermixed filamentous species, *Tribonema* sp. (cell size  $\sim 20 \times 50 \mu\text{m}$ ), and *Lyngbya* sp. (filament width  $\sim 15 \mu\text{m}$ ). Following incubation, mat sections were rinsed with buffered deionized water, placed on separate Mirr IR slides for each treatment, and dried as in the single species assessment. Prior to drying, care was taken to create a single layer of filaments as much as possible, separating filaments using forceps. Although some of the filaments still overlapped or touched other algae, many filaments were separated enough to be optically isolated with the infrared beam in the microscope.

#### Natural phytoplankton assemblage assessment

A whole water sample was collected from Cow Oak Bayou, Tunica County, Mississippi, which is a eutrophic, agriculturally influenced bayou. Water was incubated in two 50 mL clear centrifuge tubes similar to the other incubations, except no additional N or P was added. Bayou nutrient concentrations were 727  $\mu\text{g/L}$   $\text{NO}_3\text{-N}$ , 30  $\mu\text{g/L}$   $\text{NO}_2\text{-N}$ , 27  $\mu\text{g/L}$   $\text{NH}_4\text{-N}$ , 663  $\mu\text{g/L}$   $\text{PO}_4\text{-P}$ , and 7.4 mg/L DOC. Bayou alkalinity was 32 mg/L  $\text{CaCO}_3$ , pH was 6.93, and secchi depth was 8.2 cm. Each tube was amended with either 30 mg  $\text{Na}^{12}\text{CO}_3$  or  $\text{NaH}^{13}\text{CO}_3$  to attempt to alleviate C limitation. Samples were incubated for four days at 17°C (bayou water temperature) and 105  $\mu\text{mol quanta m}^{-2} \text{s}^{-1}$  PAR light intensity. Following incubation, phytoplankton were concentrated by filtering through 20 $\mu\text{m}$  mesh, rinsed into a beaker with buffered deionized water, and each treatment placed on separate Mirr IR slides. Plankton were diluted with water to produce a single layer of cells on the slide. Slides were dried at 60°C for 1 h and stored in a dark desiccator until infrared analysis. Three dominant algae were assessed; a pennate diatom (*Navicula* sp.), a colonial green alga (*Sphaerocystis* sp.), and a euglenoid (*Phacus* sp.).

### FTIR microspectroscopy

#### Benchmark

FTIR microspectroscopy of the single and two species incubations were conducted with a Bruker Hyperion 1000 infrared microscope with a liquid nitrogen cooled Mercury Cadmium Telluride infrared detector, attached to a Bruker Tensor 70 FTIR spectrometer. A 20X objective was used to visually identify target cells, and collect infrared spectra. Spectra were collected from 140 *Spirogyra* cells [70 unlabeled ( $^{12}\text{C}$ ) and 70 labeled ( $^{13}\text{C}$ )], and a minimum of 100 spectra for each *Tribonema* and *Lyngbya*, 50 unlabeled and 50 labeled

cells/filament sections. Spectra were collected in reflection-absorption mode with a wavelength resolution of  $6\text{ cm}^{-1}$ . One hundred and twenty eight scans were coadded (averaged) for *Spirogyra* and *Tribonema* per spectrum, and 256 scans coadded for *Lyngbya* due to its smaller filament width. Each scan collects infrared absorbance from  $4000\text{ cm}^{-1}$  to  $700\text{ cm}^{-1}$ , and takes approximately 1 s. Thus, spectral acquisition time was  $\sim 2$  min for each *Spirogyra* and *Tribonema* spectrum (128 scans), and  $\sim 4$  min for each *Lyngbya* spectrum (256 scans). Aperture size (the size of the hole in which infrared light is transmitted through, and, thus, the area of the cell data were collected) was  $50 \times 50\ \mu\text{m}$  for *Spirogyra* and  $15 \times 100\ \mu\text{m}$  for *Tribonema* and *Lyngbya*. Individual cells of *Lyngbya* were difficult to differentiate, so  $100\ \mu\text{m}$  filament sections were used.

Just prior to the collection of each spectra, the infrared beam's focus was checked with the OPUS FTIR software by observing the interferogram's (i.e., the pre-Fourier transformed spectra) dynamic range amplitude (i.e., signal strength). When the infrared beam is focused on the cell, the interferogram's peak amplitude is maximal, producing the strongest infrared signal. This is necessary because the microscope's visible light focus and infrared beam focus may not be matched up perfectly, and the infrared beam must be focused on the sample to provide the strongest signal to the detector. Background spectra (to correct for  $\text{CO}_2$  and water vapor infrared absorbance in the laser path, and absorbance due to any nontarget material on the slide) were collected prior to the first spectra and again after every tenth spectra. Background spectra were collected from a region on the slide within the area of the dried cell slurry, but without any visible debris. Spectra used in this study were taken only from cells that did not overlap other cells or debris and were firmly in contact with the slide. Open space between the cells and infrared reflective slide can produce unwanted infrared light scatter and give a weaker quality signal.

### Synchrotron

Due to the small size of some of the bayou phytoplankton, FTIR microspectroscopy was conducted using a synchrotron infrared source at beamline U2B at the National Synchrotron Light Source at Brookhaven National Laboratory, Upton, New York. Synchrotron infrared radiation has an approximately 1000 times greater signal to noise ratio than typical benchtop global infrared sources, and can provide better spatial resolution. This beamline was equipped with a Continuum IR microscope optically interfaced to the synchrotron through a Magna 850 FT-IR spectrometer (Thermo Fisher, Madison, Wisconsin, U.S.A.). Spectra were collected at  $4\text{ cm}^{-1}$  resolution, with 128 scans coadded. Individual spectra acquisition time were  $\sim 2$  min. Aperture size varied among species and was adjusted so the aperture fit the entire cell when possible. Due to time constraints on the

synchrotron, a minimum of 20 unlabeled and 20 labeled spectra of each species were collected.

### Spectral peak shift ( $^{13}\text{C}$ ) analysis

Spectral peak shifts due to  $^{13}\text{C}$  incorporation into cells were assessed with principal components analysis (PCA) using JMP 9.0 (SAS, Cary, North Carolina, U.S.A.). Infrared spectra are multivariate in nature and a multivariate approach such as PCA is more robust at separating samples than a univariate approach (Sackett et al. 2014). Prior to PCA analyses, raw spectra were transformed into second derivative spectra to minimize spectral differences due to baseline shifts and cell thickness (Heraud et al. 2005). Second derivative peak locations (i.e., wavenumbers) match raw spectra peaks locations, but peaks are inverted, and have a greater amplitude. Derivatives are often used to locate peaks in complex spectra (Dong et al. 1990, Kansiz et al. 1999, Sackett et al. 2014). PCA (an unsupervised method) provides a qualitative assessment of treatment differences. Principal component (PC) score plots show which PCs are important in differentiating spectra, and loading plots show specifically which spectral peaks or regions (i.e., which macromolecules) are driving spectral differences between treatments (Mariey et al. 2001).

A quantitative comparison of  $^{12}\text{C}$  and  $^{13}\text{C}$  treatment differences was done for each species using PCAToTree software (Worley et al. 2013). This program identifies 95% confidence ellipses around each PCA score cluster (i.e.,  $^{12}\text{C}$  and  $^{13}\text{C}$  groups) and provides a hypothesis test with  $p$  values for group separation using Mahalanobis distances of PC scores. Two PCs were used in calculating the confidence ellipses and  $p$  values for each species. The PCs used in this analysis were those that best separated  $^{12}\text{C}$  and  $^{13}\text{C}$  spectra, and were chosen with Discriminant Analysis (JMP 9.0) using the first ten PCs. The PCs that best separated treatments were not always those that explained the most variation among all spectra (i.e., not always PC 1 and PC 2), suggesting natural variation in cell composition can be greater than spectral changes due to  $^{13}\text{C}$  incorporation. Despite the ability to statistically test the spectral differences between  $^{12}\text{C}$  and  $^{13}\text{C}$  spectra, at this time it is not possible to accurately relate the extent of lateral peak shift to the amount of  $^{13}\text{C}$  incorporated in the cell. Therefore, this method is currently only a qualitative estimate of  $^{13}\text{C}$  incorporation.

## Assessment

### Single species incubation

Incubating algae in  $^{13}\text{C}$  caused lateral peak shifts throughout *Spirogyra* spectra. The mean raw spectrum showed peak shifts in the two main regions where C containing molecules are observed,  $3100\text{--}2850\text{ cm}^{-1}$  and  $1800\text{--}750\text{ cm}^{-1}$  (Table 1; Fig. 1a). Specifically,  $^{13}\text{C}$  caused a lateral, downward (lower wavenumber) shift in  $\text{CH}_2/\text{CH}_3$  groups in the  $3100\text{--}2850\text{ cm}^{-1}$  region (Fig. 1b). These peaks are often assigned

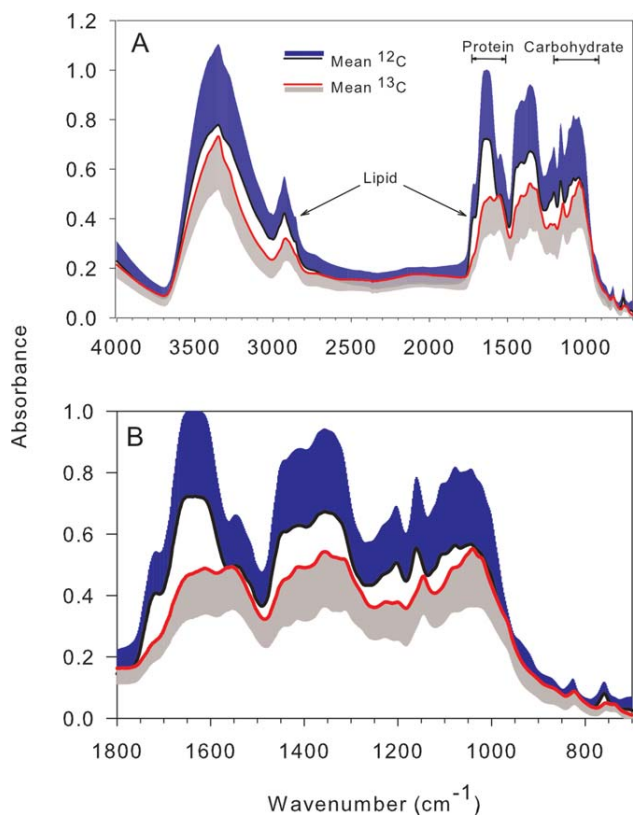


**Fig. 1.** Single species incubation. (A) Average  $^{12}\text{C}$  carbon (black line, blue 1 SD,  $n = 70$ ) and  $^{13}\text{C}$  carbon (red line, gray 1 SD,  $n = 70$ ) spectra of *Spirogyra* sp. Only positive or negative standard deviations are shown for each mean to increase spectral clarity. Major peaks or regions for lipids, proteins, and carbohydrates are labeled. (B) 1800–700  $\text{cm}^{-1}$  region where the majority of biochemical information is found. Peaks impacted by  $^{13}\text{C}$  incorporation (red spectrum) have a lateral shift to a right (lower wavenumber) as compared to the  $^{12}\text{C}$  peaks (black spectrum).

to the fatty acid methyl and methylene groups of lipids but also can be caused by  $\text{CH}_2/\text{CH}_3$  groups in other macromolecules. The lipid ester carbonyl ( $\text{C}=\text{O}$ ) peak at  $\sim 1720 \text{ cm}^{-1}$  was also reduced. The major protein peak regions [amide I ( $\text{C}-\text{O}$ ) and amide II ( $\text{C}-\text{N}$ ), 1710–1560  $\text{cm}^{-1}$ ], and carbohydrate regions ( $\text{C}-\text{O}$  and  $\text{C}-\text{O}-\text{C}$ , 1200–900  $\text{cm}^{-1}$ ) also had downward peak shifts (Fig. 1b).

Second derivative spectra showed distinct lateral peak shifts in  $^{13}\text{C}$  spectra in regions that represent C containing macromolecules (Fig. 2). Lipids were likely impacted, as there was a widening of the 2928  $\text{cm}^{-1}$  methylene peak, and shift of the 2850  $\text{cm}^{-1}$  methyl/methylene peak to 2845  $\text{cm}^{-1}$  (Fig. 2a). Proteins peak shifts occurred, but lateral movement of these peaks were more complex (Fig. 2b). The amide I peak at 1671  $\text{cm}^{-1}$  widened, created by shifts to 1655  $\text{cm}^{-1}$ , and a large shift down to 1611  $\text{cm}^{-1}$ . The amide II peak at 1600  $\text{cm}^{-1}$  shifted downward 25  $\text{cm}^{-1}$  to 1575  $\text{cm}^{-1}$ , which is within the theoretical peak shift of  $^{13}\text{C}$  replacement of a  $\text{C}-\text{O}$  molecule (Supporting Information Table S1).

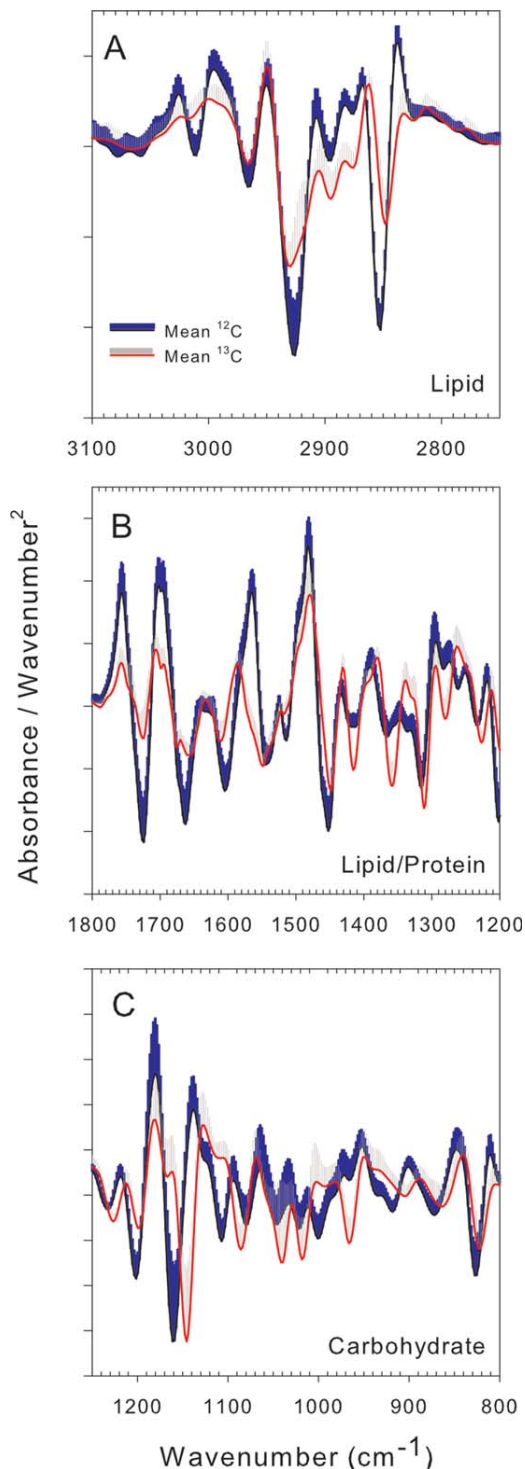


**Fig. 2.** *Spirogyra* second derivative mean spectra. Mean  $^{12}\text{C}$  carbon (black line, blue 1 SD,  $n = 70$ ) and  $^{13}\text{C}$  carbon (red line, gray 1 SD,  $n = 70$ ) spectra of *Spirogyra* sp. Only positive standard deviations are shown to increase spectral clarity. Lateral peak shifts occurred in A) lipid peaks at 2928  $\text{cm}^{-1}$  and 2845  $\text{cm}^{-1}$ , B) protein peaks at 1671  $\text{cm}^{-1}$ , 1655  $\text{cm}^{-1}$ , and 1600  $\text{cm}^{-1}$ , and C) all carbohydrate peaks. Note second derivative peaks point downward.

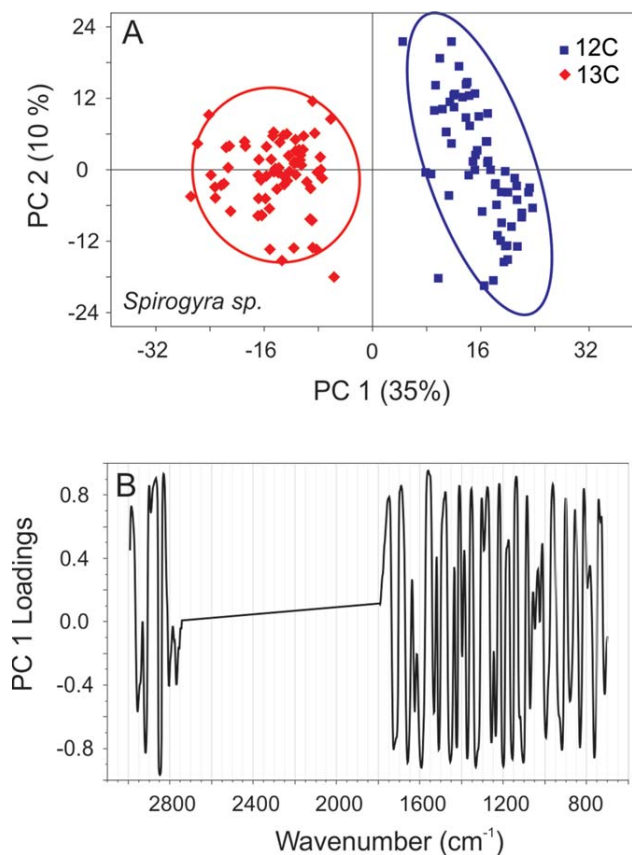


**Fig. 3.** *Spirogyra* spectra comparison between treatments. (A) Principal component analysis on  $^{12}\text{C}$  (blue) and  $^{13}\text{C}$  (red) spectra. Each point is a spectra from unique cells. Ellipses are 95% confidence intervals of group location based on PC scores. (B) PC 1 loading plot showing how spectra differ. Negative peaks correspond to peaks in  $^{12}\text{C}$  spectra that shifted due to isotope incorporation.

Substantial  $^{13}\text{C}$  was incorporated into carbohydrates as each peak from  $1200\text{ cm}^{-1}$  to  $900\text{ cm}^{-1}$  had noticeable lateral shifts (Fig. 2c). Peak shifts away from  $1160\text{ cm}^{-1}$ ,  $1108\text{ cm}^{-1}$ ,  $1080\text{ cm}^{-1}$ ,  $1048\text{ cm}^{-1}$ , and  $1030\text{ cm}^{-1}$  suggests *Spirogyra* was putting C into cellulose (Table 1). As predicted, most observed lateral peak shifts were not as great as theoretical shifts (Supporting Information Table S1), but most peaks that correspond to C containing molecules did exhibit consistent lateral shifts.

Shifts in second derivative peaks appeared complex at times, as with the amide I peak at  $\sim 1660\text{ cm}^{-1}$  and the amide II peak at  $\sim 1600\text{ cm}^{-1}$  in Fig. 2b. The  $^{13}\text{C}$  amide I peak has a doublet located on either side of the  $^{12}\text{C}$  peak. Also, the amide II  $^{13}\text{C}$  peak appears to be shifted left of the  $^{12}\text{C}$  peak. This may be due to the complexity of these two protein peaks, as each of these peaks are made up of a combination of several different bonds each absorbing specific infrared wavelengths very near one another. Some of these bonds have different shift distances with  $^{13}\text{C}$ , and

some do not contain C atoms and, thus, have no shift. For example, the amide I peak is mostly due to C=O bond absorption, but can also include C=C bond absorption, while the amide II peak is made up of a combination of C—O, C—N, and N—H bond absorptions. Peak doublets can likely be made as  $^{13}\text{C}$  incorporated into selective cellular proteins causes some peaks to shift, but leaving others, as in the amide I peak. In the amide II peak, it appears isotope replacement in the C—O bond was significant, causing a very large shift to the right (down to  $1575\text{ cm}^{-1}$ , which is still within the theoretical calculated movement of this bond). However, some peaks that make up the amide II, perhaps the N—H bond (which can absorb infrared wavelengths above  $1600\text{ cm}^{-1}$ ) did not shift, leaving what appears to be a smaller left-shifted amide II peak.

#### PCA

The PCA of *Spirogyra* spectra distinctly separated cells from  $^{12}\text{C}$  and  $^{13}\text{C}$  treatments along the first PC axis, which explained 35% of overall spectral variation (Fig. 3a). This PC1 separation suggests spectral variability was greater between isotope treatments than among cells within a treatment. Each mark on the PCA biplot represents a single *Spirogyra* cell. All  $^{13}\text{C}$  cells were outside of the  $^{12}\text{C}$  treatment 95% confidence interval, and the two groups were significantly separated ( $p < 0.001$ ) based on PC score Mahalanobis distances. The PC 1 loading plot (Fig. 3b) shows where  $^{12}\text{C}$  and  $^{13}\text{C}$  spectra differ.  $^{12}\text{C}$  spectra have positive associations with PC 1 so the negative peaks in the loading plot correspond to second derivative peaks that are in the  $^{12}\text{C}$  spectra, but not the  $^{13}\text{C}$  spectra. Thus, positive peaks correspond to second derivative peaks that occur in the  $^{13}\text{C}$  spectra, but not the  $^{12}\text{C}$  spectra. This relationship is because the PCA was done on second derivative spectra where the molecular information is gained from negative peaks. Each prominent peak shift in the second derivative mean spectra (Fig. 2) corresponds to a prominent peak in the PC 1 loading plot (Fig. 3b). For example, nearly all of the  $^{12}\text{C}$  peaks that had large shifts in Fig. 2 (e.g.,  $2850\text{ cm}^{-1}$ ,  $1450\text{ cm}^{-1}$ ,  $1370\text{ cm}^{-1}$ ,  $1200\text{ cm}^{-1}$ ,  $1160\text{ cm}^{-1}$ ,  $1110\text{ cm}^{-1}$ , and  $920\text{ cm}^{-1}$ ) have corresponding large negative peaks in the PC 1 loading plot. This peak correspondence suggests group separation along this PC axis was largely due to isotope incorporation.

#### Two-species incubation

*Lyngbya* and *Trebonema* second derivative spectra each had lateral peak shifts due to  $^{13}\text{C}$  incubation (Fig. 4), but lipid, protein, and carbohydrate peak shifts were unique in each species. Neither species had large lipid peak shifts,  $\sim 2970\text{ cm}^{-1}$  to  $2850\text{ cm}^{-1}$ , and  $1740\text{ cm}^{-1}$ , although *Lyngbya* had slightly larger shifts (Fig. 4a,d). *Lyngbya* and *Trebonema* both had a  $10\text{ cm}^{-1}$  shift in the amide I protein peak at  $\sim 1650\text{ cm}^{-1}$ , but a shift in the amide II peak at  $\sim 1550\text{ cm}^{-1}$  was only observed in *Lyngbya* (Fig. 4b,e). Both species had substantial shifts in carbohydrate peaks from

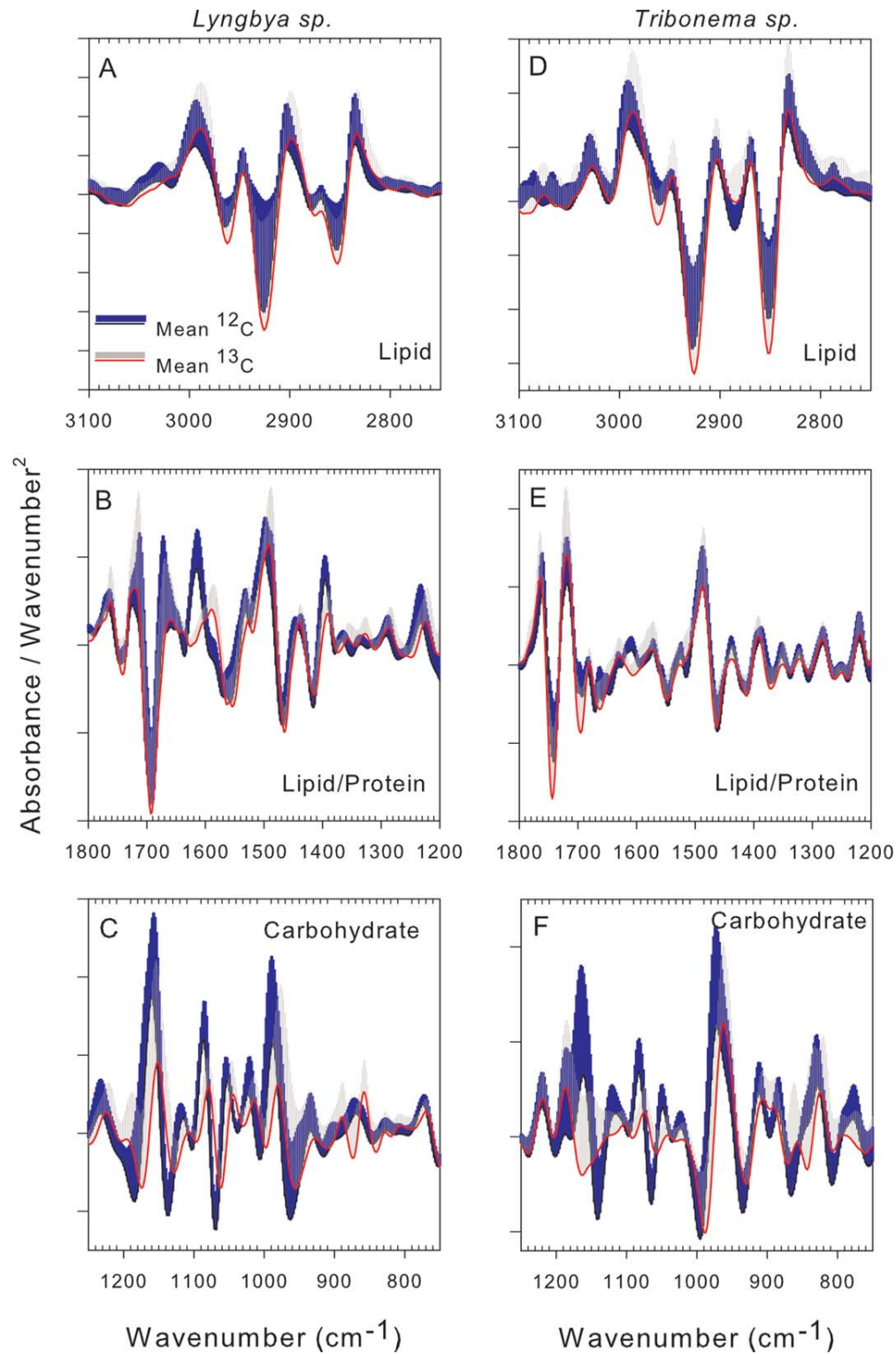


**Fig. 4.** Two species incubation. Mean second derivative spectra of *Lyngbya* (A–C) and *Tribonema* (D–F); <sup>12</sup>carbon (black line, blue 1 SD,  $n = 50$ ) and <sup>13</sup>carbon (red line, gray 1 SD,  $n = 50$ ). Only positive standard deviations are shown to increase spectral clarity. (A and D) Lipid peak shifts, (B and E) Lipid/protein peak shifts, and (C and F) carbohydrate peak shifts following <sup>13</sup>carbon incorporation. Note second derivative peaks point downward.

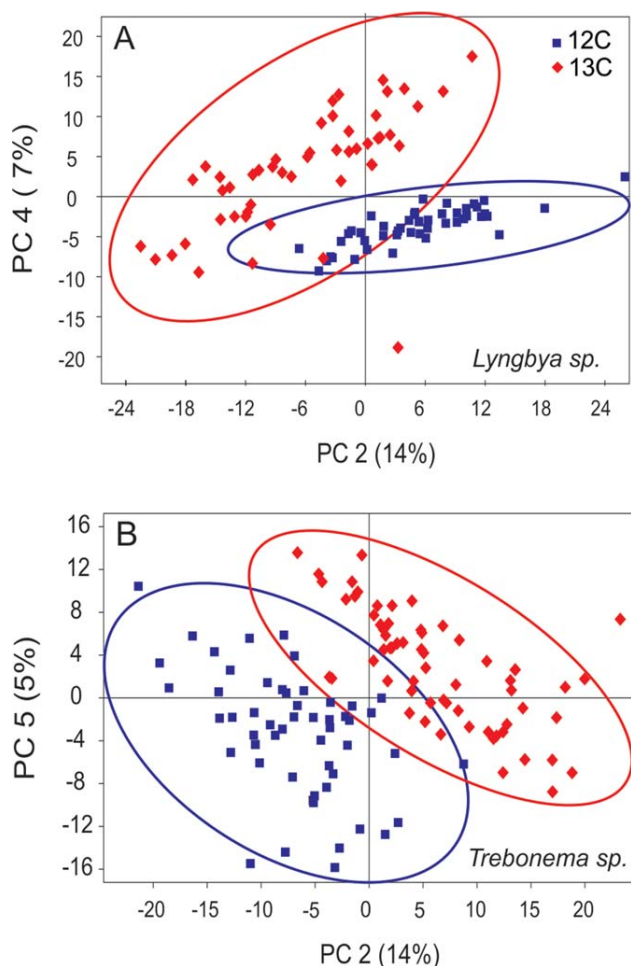


**Fig. 5.** Two species incubation comparisons between isotope treatments. (A) *Lyngbya* principal component analysis on  $^{12}\text{C}$  (blue) and  $^{13}\text{C}$  (red) treatments. (B) *Trebonema* principal component analysis on  $^{12}\text{C}$  and  $^{13}\text{C}$  carbon treatments. Points are spectra from unique cells and ellipses are 95% confidence intervals of group location based on PC scores.

$1200\text{ cm}^{-1}$  to  $900\text{ cm}^{-1}$  (Fig. 4c,f). Given these peak shifts, the cyanobacterium *Lyngbya* incorporated more of the  $^{13}\text{C}$  into carbohydrates and proteins, and some into lipids, while *Trebonema* put more of the  $^{13}\text{C}$  into carbohydrates and some into proteins.

#### PCA

*Lyngbya* and *Trebonema* PCAs both had distinct and significant treatment separations (*Lyngbya*  $p < 0.001$ , and *Trebonema*  $p < 0.001$ , Fig. 5a,b). Unlike *Spirogyra*, the PCs that best separated treatments were not those that explained the most variation among spectra, that is, not PC 1. PCs 2 (14.2%) and 4 (6.7%) best separated *Lyngbya* isotope treatments, and PCs 2 (13.9%) and 5 (5.3%) best separated *Trebonema* isotope treatments. Although intercellular variations within each of these species were greater than spectral changes due to  $^{13}\text{C}$  incorporation because isotope treatments were not separated

by PC 1, isotope incorporation was still observed by the next PC, that is, PC 2.

PC loading plots showed each prominent peak shift in the *Lyngbya* second derivative mean spectra (Fig. 4a-c) corresponds to a prominent peak in the PC 2 or PC 4 loading plot (Supporting Information Fig. S1a,b). All of the  $^{12}\text{C}$  peaks that had large shifts have corresponding large negative peaks in the PC loading plots. PC 2 contained peaks that corresponded to proteins peaks at  $1637\text{ cm}^{-1}$ ,  $1415\text{ cm}^{-1}$ ,  $1375\text{ cm}^{-1}$ ,  $1348\text{ cm}^{-1}$ , and  $1267\text{ cm}^{-1}$ , and carbohydrate peaks at  $1186\text{ cm}^{-1}$ ,  $1068\text{ cm}^{-1}$ ,  $1039\text{ cm}^{-1}$ ,  $964\text{ cm}^{-1}$ , and  $914\text{ cm}^{-1}$ . PC 4 contained peaks that corresponded to lipids at  $2968\text{ cm}^{-1}$ ,  $2929\text{ cm}^{-1}$ ,  $2879\text{ cm}^{-1}$ , and  $1747\text{ cm}^{-1}$ , proteins at  $1558\text{ cm}^{-1}$ ,  $1467\text{ cm}^{-1}$ , and  $1315\text{ cm}^{-1}$ , and carbohydrates at  $1137\text{ cm}^{-1}$ ,  $1103\text{ cm}^{-1}$ , and  $1006\text{ cm}^{-1}$ .

Negative peaks in PC loading plots also corresponded to second derivative peak shifts in *Trebonema* cells. PC 2 loadings contained most of the shifted peaks with  $^{12}\text{C}$  lipid peaks at  $2929\text{ cm}^{-1}$ ,  $2856\text{ cm}^{-1}$ , and  $1737\text{ cm}^{-1}$ , protein peaks at  $1672\text{ cm}^{-1}$ ,  $1415\text{ cm}^{-1}$ , and  $1375\text{ cm}^{-1}$ , and carbohydrate peaks at  $1095\text{ cm}^{-1}$ ,  $1066\text{ cm}^{-1}$ ,  $997\text{ cm}^{-1}$ , and  $867\text{ cm}^{-1}$  (Supporting Information Fig. S1c). PC 5 contained peaks that corresponded to a lipid peak at  $2656\text{ cm}^{-1}$ , and carbohydrate peaks at  $937\text{ cm}^{-1}$  and  $898\text{ cm}^{-1}$  (Supporting Information Fig. S1d).

#### Natural phytoplankton assemblage

Bayou phytoplankton spectra had varying degrees of peak shifts following  $^{13}\text{C}$  incubation. The diatom *Navicula* (Fig. 6a) had larger lateral peak shifts than the green alga *Sphaerocystis* (Fig. 6b) or the euglenoid *Phacus* (Fig. 6c). Spectral shifts showed the diatom incorporated more C into proteins and carbohydrates than lipids. The largest protein peak shifts in *Navicula* occurred in the amide I protein peak moving from  $1623\text{ cm}^{-1}$  to  $1602\text{ cm}^{-1}$ , the  $\text{CH}_2/\text{CH}_3$  peak that is often assigned to proteins and carbohydrates in this region, moved from  $1252\text{ cm}^{-1}$  to  $1233\text{ cm}^{-1}$ . Every peak in the carbohydrate region from  $1200\text{ cm}^{-1}$  to  $900\text{ cm}^{-1}$  also shifted to the right. Smaller shifts in lipid peaks (methyl/methylene peaks at  $2954\text{ cm}^{-1}$  and  $2848\text{ cm}^{-1}$ , and the carbonyl peak at  $1737\text{ cm}^{-1}$ ) were observed.

*Sphaerocystis* and *Phacus* spectral peak locations did not change as much as in the diatom, suggesting these species did not incorporate as much  $^{13}\text{C}$ . In *Sphaerocystis*, the largest peak shifts occurred in the amide I protein peak moving from  $1626\text{ cm}^{-1}$  to  $1610\text{ cm}^{-1}$ , with multiple smaller shifts associated with proteins moving away from  $1420\text{ cm}^{-1}$  to  $1240\text{ cm}^{-1}$ . A large shift occurred in a carbohydrate peak, moving from  $1198\text{ cm}^{-1}$  to  $1185\text{ cm}^{-1}$ , but there was some discontinuity between the derivative spectra of each treatment from  $1166\text{ cm}^{-1}$  to  $994\text{ cm}^{-1}$  that made peak shift interpretation difficult for the carbohydrate region. Minimal peak shifts were observed in the  $3050\text{ cm}^{-1}$  to  $2800\text{ cm}^{-1}$  lipid range, and no shift in the  $1745\text{ cm}^{-1}$

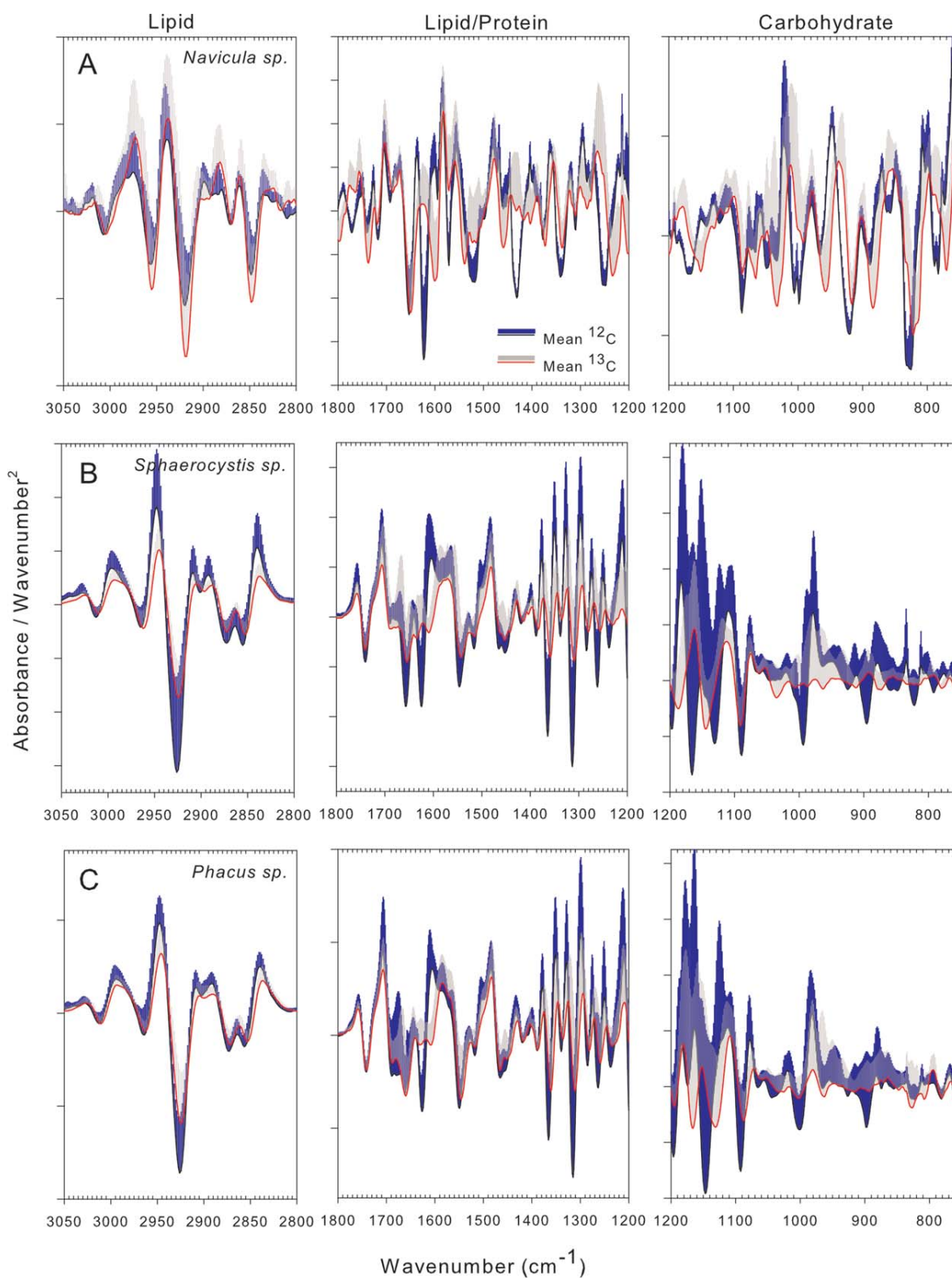


**Fig. 6.** Natural phytoplankton assemblage mean second derivative spectra for (A) *Navicula*, (B) *Sphaerocystis*, and (C) *Phacus*. Mean <sup>12</sup>carbon (black line, blue 1 SD) and <sup>13</sup>carbon (red line, gray 1 SD) spectra. Only positive standard deviations are shown to increase spectral clarity. Note second derivative peaks point downward.

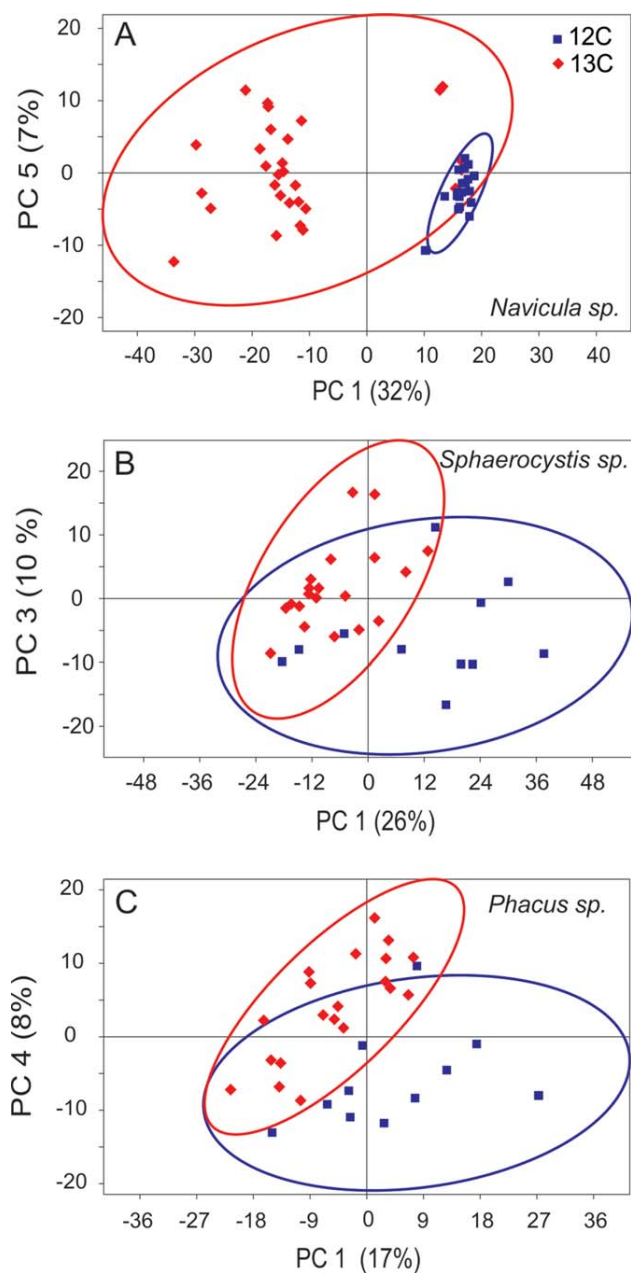


**Fig. 7.** Natural phytoplankton assemblage comparisons between isotope treatments. Principal component analysis on  $^{12}\text{C}$  (blue) and  $^{13}\text{C}$  (red) treatments for (A) *Navicula*, (B) *Sphaerocystis*, and (C) *Phacus*. Points are spectra from unique cells and ellipses are 95% confidence intervals of group location based on PC scores.

major lipid peak. *Phacus* had similar peak shifts as *Sphaerocystis* in all regions (Fig. 6b,c). There was a noticeable decrease in the dominant protein peak at  $1626\text{ cm}^{-1}$  suggesting some replacement of the C in the C=O amide bonds in proteins. There were also slight shifts away from protein related peaks at  $1365\text{ cm}^{-1}$ ,  $1315\text{ cm}^{-1}$ ,  $1284\text{ cm}^{-1}$ ,  $1264\text{ cm}^{-1}$ , and  $1238\text{ cm}^{-1}$ . Carbohydrate peaks shifts were

evident, moving away from  $1170\text{ cm}^{-1}$ ,  $1146\text{ cm}^{-1}$ , and  $1090\text{ cm}^{-1}$  (Fig. 6c). Like *Sphaerocystis*, *Phacus* had minimal lipid peak shifts in the  $3050\text{ cm}^{-1}$  to  $2800\text{ cm}^{-1}$  range and at  $1740\text{ cm}^{-1}$ .

#### PCA

Bayou phytoplankton PC scores were not as well divided by treatments as the earlier incubations, but based on relative group separation, the diatom incorporated more  $^{13}\text{C}$  than the other two species (Fig. 7). Also, all species' PCA biplots that showed the greatest treatment group separations included PC 1. Thus,  $^{13}\text{C}$  incorporation had substantial and consistent influence on each species' spectra. *Navicula* treatments differed significantly ( $p < 0.001$ ) along PC 1 (32%, Fig. 7a). All but five  $^{13}\text{C}$  spectra (i.e., five diatom cells) appeared to be sufficiently labeled to separate along PC 1. The PC loading plot showed spectral differences were driven by  $^{13}\text{C}$  spectra having a lipid peak at  $1771\text{ cm}^{-1}$ , protein peaks at  $1430\text{ cm}^{-1}$ ,  $1350\text{ cm}^{-1}$ , and  $1252\text{ cm}^{-1}$ , and carbohydrate peaks at  $1181\text{ cm}^{-1}$ ,  $926\text{ cm}^{-1}$ , and  $831\text{ cm}^{-1}$  (Supporting Information Fig. S2a,2b). Note when interpreting these loading plots that spectra from *Navicula*  $^{12}\text{C}$  treatments were positively associated with PC 1, and  $^{13}\text{C}$  spectra correlate with the negative PC 1 loadings.

*Sphaerocystis* and *Phacus* PC scores were not as well separated as *Navicula*, but still showed distinct treatment groupings, with changes seen in proteins, lipids, and carbohydrates. *Sphaerocystis* treatment separation was significant on PCs 1 and 3 ( $p < 0.001$ ). PC 1 (26%) was distinguished by  $^{12}\text{C}$  spectra lipid peaks at  $2928\text{ cm}^{-1}$  and  $2877\text{ cm}^{-1}$ , and protein peaks at  $1363\text{ cm}^{-1}$ ,  $1313\text{ cm}^{-1}$ ,  $1283\text{ cm}^{-1}$ ,  $1261\text{ cm}^{-1}$ , and  $1240\text{ cm}^{-1}$  (Supporting Information Fig. S2c). PC 3 (10%) was distinguished by protein peaks at  $1679\text{ cm}^{-1}$ ,  $1415\text{ cm}^{-1}$ , and  $1384\text{ cm}^{-1}$ , and carbohydrate peaks at  $1190\text{ cm}^{-1}$ ,  $947\text{ cm}^{-1}$ , and  $874\text{ cm}^{-1}$  (Supporting Information Fig. S2d). *Phacus* spectra from the two isotope treatments were moderately well separated with PCA, with PCs 1 and 4 providing the best treatment separation (Fig. 7c). Despite overlap of the 95% confidence intervals, PCA treatment separations were significantly different ( $p < 0.001$ ). PC 1 (17%) was characterized by shifts in protein peaks at  $1367\text{ cm}^{-1}$ ,  $1318\text{ cm}^{-1}$ , and  $1286\text{ cm}^{-1}$ , and carbohydrate peaks at  $1198\text{ cm}^{-1}$ ,  $1091\text{ cm}^{-1}$ , and  $1005\text{ cm}^{-1}$  (Supporting Information Fig. S2e). PC 4 (8%) was defined by lipid related peak shifts at  $2913\text{ cm}^{-1}$ ,  $2847\text{ cm}^{-1}$ , and  $1753\text{ cm}^{-1}$ , protein peak shifts at  $1606\text{ cm}^{-1}$  and  $1280\text{ cm}^{-1}$ , and unknown peak shifts at  $809\text{ cm}^{-1}$  and  $775\text{ cm}^{-1}$  (Supporting Information Fig. S2f).

#### Discussion

Fourier-transform infrared microspectroscopy is a well-established technique for assessing the chemical distribution of single algal cells (Beardall et al. 2001; Heraud et al. 2005;

Giordano et al. 2009). Although FTIR spectroscopy is a label-free technique, adding  $^{13}\text{C}$  isotope as a tracer provides a qualitative method to track C incorporation in individual algal cells.  $^{13}\text{C}$  Carbon labeling allows the determination of which species within a natural, multispecies community are incorporating inorganic C (i.e.,  $\text{CO}_2$  or  $\text{H}_2\text{CO}_3$ ), and could also potentially detect labeled organic C uptake. Additionally, by detecting lateral shifts in spectral peaks that correspond to specific molecular compounds, this method can assess which major macromolecules the cell is making with the newly incorporated C. Thus, FTIR isotopic labeling links cell physiology to the functional roles of each species, and paves the way for more explicit tests of the diversity/functional relationships in microalgal communities than currently possible (e.g., Cardinale 2011).

The three incubation assessments provided clear evidence that spectral peak shifts occurred due to isotope labeling, and that these peak shifts can be detected within individual cells or species in mixed-species assemblages. These assessments included representatives of cyanobacteria, diatoms, chlorophytes, euglenoids, and xanthophytes showing that isotope tracking is possible across diverse groups of algae. The algal groups used did however have varying spectral changes following incubations. For example, *Spirogyra* had the largest peak shifts, and the one and two species incubations had larger peak shifts than the natural assemblage. Perhaps *Spirogyra* incorporated more  $^{13}\text{C}$  due to a lack of competition in a one species incubation, but a more detailed assessment is needed to verify this mechanism. The length of incubation time will also impact peak shift magnitude as larger shifts should occur as more isotope is incorporated into cell material. The one and two species incubations were run for longer than the natural assemblage, which most likely allowed for more time to incorporate  $^{13}\text{C}$  into cells. This time difference may have also accounted for decreased PCA treatment separations of species from the natural assemblage. For the first two incubations, longer incubation times were used to ensure cells were adequately labeled with isotope; however, shorter incubation lengths in the bayou phytoplankton showed that diatoms may have been assimilating C more efficiently, or growing faster than the other two species.

Incubations were short enough that complete replacement of cell material with  $^{13}\text{C}$  did not occur as species-specific trends in  $^{13}\text{C}$  incorporation were observed within the multispecies incubation. Most notably, each species used the new C for different macromolecules, and the magnitude of peak shifts (i.e.,  $^{13}\text{C}$  incorporation) varied among co-occurring species. For example, the *Lyngbya/Trebonema* incubation showed that *Lyngbya* put more new C into carbohydrates and lipids (energy storage products), while *Trebonema* put more new C into proteins (cell growth and metabolism products) in addition to some carbohydrates.

The use of PCA of second derivative spectra to group algal cells by treatments is well established, and has been used to classify algal spectra (i.e., cell biochemistry) based on environmental differences such as nutrient limitation (Sigeo et al. 2007),  $\text{CO}_2$  uptake (Domenighini and Giordano 2009), and herbicide impacts (Murdock and Wetzel 2012). Within the natural assemblage, stronger PC separation of the diatom suggests they were taking in more  $^{13}\text{C}$  than the green algae or euglenoids. This agrees with previous work that has shown diatom RubisCO has the highest affinity for  $\text{CO}_2$  of any group of algae (Tortell et al. 2000), and that euglenoids can use organic C when it is in high concentrations (Sanders and Porter 1988; Yamane et al. 2001), such as in the eutrophic bayou. Some  $^{13}\text{C}$  was likely respired during the incubations, and this can impact relative comparisons among species if macromolecule biomass turns over at different rates. Shorter incubation times or time series analysis during incubations may minimize this issues.

Carbon shifts are substantially greater and occur in more peaks along a spectrum than peak shifts found in  $^{15}\text{N}$  Nitrogen isotope uptake in the green alga *Cladophora glomerata* (Murdock et al. 2008). Whereas notable  $^{15}\text{N}$ -mediated shifts occurred in only the amide I and amide II protein regions,  $^{13}\text{C}$  shifts in the present study were evident throughout the spectrum and, thus, can be used to assess cellular carbohydrates and lipids in addition to protein. Combined C and N isotope labeling and FTIR analysis has been done previously to study photosystem II structure (Noguchi and Sugiura 2003) and this dual isotope method could provide even more information regarding how stoichiometric changes in the environment impact algal cellular nutrient uptake and allocation.

FTIR microspectroscopy has two important limitations for algal biochemical analyses, a relatively large minimum cell size, and only qualitative isotope detection. Microalgal cells range in size from approximately  $2\ \mu\text{m}$  to  $200\ \mu\text{m}$ , and small algal cells (picoplankton,  $\sim 2\ \mu\text{m}$ ) can be ecologically important (Richardson and Jackson 2007; Moran et al. 2010). However, most FTIR accessible instruments (benchtop FTIR spectrometers with a global infrared source) have a practical spatial resolution of  $\sim 20\ \mu\text{m}$ . Global infrared sources do provide adequate signal to noise ratio for whole cells greater than approximately  $20\ \mu\text{m}$  and subcellular resolution of larger algae. Synchrotrons provide an infrared source approximately 1000 times brighter than global sources, which give much greater signal to noise output, and a minimum reliable spatial resolution of approximately  $5\ \mu\text{m}$  to  $10\ \mu\text{m}$ . FTIR spatial resolution is improving as Nasse et al. (2011) have achieved subwavelength diffraction-limited resolution using multibeam synchrotron imaging. Spatial resolution in benchtop equipment is also improving with advances in attenuated total reflectance (ATR) objectives and quantum cascade (QC) lasers. These adaptations can provide spatial resolution near wavelength diffraction-limited resolution

(i.e., resolution is limited to the size of the infrared wavelength used) in the mid-infrared region (wavelengths from 2.5 – 13.0  $\mu\text{m}$ , 4000  $\text{cm}^{-1}$  to 769  $\text{cm}^{-1}$ ). However, there are still limitations with ATR objectives and QC lasers that can hinder algal analyses. ATR objectives only penetrate a few micrometers into the cell, which may be adequate for smaller cells, but this can limit its application to larger cells and three-dimensional colonies. Current commercially available QC lasers have a limited wavelength range in the mid-infrared (5.4 – 12.8  $\mu\text{m}$ , 1851  $\text{cm}^{-1}$  to 781  $\text{cm}^{-1}$ ), but this range does include prominent lipid, protein, and carbohydrate peaks. Despite the size limitation imposed by limited accessibility of synchrotron sources, many important algal species can still be adequately assessed with readily available benchtop equipment. This methodology can also be applied without a microscope by making a pellet from a mass of many cells, if only community level C uptake information is needed.

It is not currently possible to measure the mass of isotope in cells using FTIR spectroscopy. Quantification is difficult using the magnitude of lateral peak shift because several molecular bonds can contribute to each peak, and a single molecule bond type (e.g., C–H, C–O, or C=O) can contribute to more than one peak. Also, different C-containing molecules have varying maximum peak shifts with complete isotopic substitution (Supporting Information Table S1). Quantification of components in infrared spectra are typically made by creating calibration curves using pure components of interest and then comparing spectra of known substances with that of individual specimens using multivariate analyses such as partial least squares regression or principal component regression (Horton et al. 2011). This approach cannot easily be used with isotope labeling because the label causes shifts in peaks already present, and not the creation of new peaks. Further steps to quantify  $^{13}\text{C}$  uptake with this method would require the comparison of spectra from a range of  $^{13}\text{C}$  diluted and replete cells. Nevertheless, the magnitude of the lateral shift in peak position can provide qualitative estimates of competitive uptake ability among species or individuals in a population, as larger downward shifts correspond to greater  $^{13}\text{C}$  uptake. Despite the qualitative nature of this method, the ability to detect differences in C incorporation among cells, and distribution of newly acquired C into cell macromolecules provides a new avenue of in situ, mixed-species understanding of algal competition, C sequestration, and environmental adaptation.

### Comments and recommendations

Biological samples are inherently complex and exhibit relatively high infrared spectral variation compared to non-biological samples. For example, second derivative spectra were necessary to account for variation in sample (i.e., cell) thickness and potential spectral baseline variation due to reso-

nant Mie scattering with small cells (Bassan et al. 2010). Additionally,  $^{13}\text{C}$  incorporation spectral changes were at times overshadowed by cell-to-cell biochemical variation, for example, *Lyngbya* and *Trebonema* treatments were not separated along PC 1. It was anticipated that spectral differences due to macromolecular content would be greater than isotope shifts as the largest peaks are dependent on a cell's chemical composition. These differences however are mainly due to changes in peak height, while isotope changes cause lateral shifts in peaks. The PCA approach of spectra differentiation uses discrete orthogonal components, and appears to be able to separate out isotope induced changes in spectra quite well, just not always on the first few PC axes. That said, the separation between treatments was much more distinct in the one and two species incubations than from the natural assemblage (where algae potentially could have had more individual macromolecular variation). Further testing of different multivariate and ordination techniques may be able to better pinpoint lateral vs. vertical peak shifts. Notwithstanding significant cell variation, the observed distinct spectral changes attributed to  $^{13}\text{C}$  uptake in all algal species suggested this technique can be widely used across algal species and habitats.

Currently, understanding how an algal species responds to external changes involves growing it in a single-species laboratory culture to generate enough biomass (milligrams to grams) to run standard biochemical tests. Biochemical assessments and competition experiments are, thus, limited to a few species in culture, or to enumerating community composition changes in multispecies assemblages. This FTIR isotope labeling method is quicker, can measure species-specific in-situ responses, and can assess C uptake and allocation variation at the population, individual alga, and subcellular scale. Potential applications of this technique include ecological research such as algal competition, resource use, or elucidating microbial nutrient pathways, as well as algal biotechnology applications including species selection for optimal biofuel production or pollutant treatment systems. Additionally this technique can be easily applied to other microorganisms such as bacteria, fungi, or zooplankton; and potentially modified to look at C incorporation into tissues of larger plants and animals.

### References

- Bassan, P., and others. 2010. Resonant Mie Scattering (RMieS) correction of infrared spectra from highly scattering biological samples. *Analyst*. **135**: 268–277. doi:10.1039/b921056c
- Beardall, J., and others. 2001. A comparison of methods for detection of phosphate limitation in microalgae. *Aquat. Sci.* **63**: 107–121. doi:10.1007/PL00001342
- Behl, S., A. Donval, and H. Stibor. 2011. The relative importance of species diversity and functional group diversity on

- carbon uptake in phytoplankton communities. *Limnol. Oceanogr.* **56**: 683–694. doi:10.4319/lo.2011.56.2.0683
- Cardinale, B. J. 2011. Biodiversity improves water quality through niche partitioning. *Nature*. **472**: 86–89. doi:10.1038/nature09904
- Corcoran, A. A., and W. J. Boeing. 2012. Biodiversity increases the productivity and stability of phytoplankton communities. *PLoS One*: e49397. doi:10.1371/journal.pone.0049397
- Dean, A. P., J. M. Nicholson, and D. C. Sigee. 2008. Impact of phosphorus quota and growth phase on carbon allocation in *Chlamydomonas reinhardtii*: An FTIR microspectroscopy study. *Eur. J. Phycol.* **43**: 345–354. doi:10.1080/09670260801979287
- Dean, A. P., and D. C. Sigee. 2006. Molecular heterogeneity in *Aphanizomenon flos-aquae* and *Anabaena flos-aquae* (Cyanophyta): A synchrotron-based Fourier-transform infrared study of lake micropopulations. *Eur. J. Phycol.* **41**: 201–212. doi:10.1080/09670260600645907
- Domenighini, A., and M. Giordano. 2009. Fourier Transform Infrared spectroscopy of microalgae as a novel tool for biodiversity studies, species identification, and the assessment of water quality. *J. Phycol.* **45**: 522–531. doi:10.1111/j.1529-8817.2009.00662.x
- Dong, A., P. Huang, and W. S. Caughey. 1990. Protein secondary structures in water from second-derivative amide I infrared spectra. *Biochemistry* **29**: 3303–3308. doi:10.1021/bi00465a022
- Esler, M., D. Griffith, S. Wilson, and L. Steele. 2000. Precision trace gas analysis by FT-IR spectroscopy. 2. The  $^{13}\text{C}/^{12}\text{C}$  isotope ratio of  $\text{CO}_2$ . *Anal. Chem.* **72**: 216–221. doi:10.1021/ac990563x
- Falkowski, P., and others. 2000. The global carbon cycle: A test of our knowledge of earth as a system. *Science* **290**: 291–296. doi:10.1126/science.290.5490.291
- Giordano, M., M. Kansiz, P. Heraud, J. Beardall, B. Wood, and D. McNaughton. 2001. Fourier transform infrared spectroscopy as a novel tool to investigate changes in intracellular macromolecular pools in the marine microalga *Chaetoceros muellerii* (Bacillariophyceae). *J. Phycol.* **37**: 271–279. doi:10.1046/j.1529-8817.2001.037002271.x
- Giordano, M., and S. Ratti. 2013. The biomass quality of algae used for  $\text{CO}_2$  sequestration is highly species-specific and may vary over time *J. Appl. Phycol.* **25**: 1431–1434. doi:10.1007/s10811-012-9966-2
- Giordano, M., S. Ratti, A. Domenighini, and F. Vogt. 2009. Spectroscopic classification of 14 different microalga species: First steps towards spectroscopic measurement of phytoplankton biodiversity **2**: 155–164. doi:10.1080/17550870903353088
- Heraud, P., S. Caine, G. Sanson, R. Gleadow, B. R. Wood, and D. McNaughton. 2007. Focal plane array infrared imaging: A new way to analyse leaf tissue. *New Phytol.* **173**: 216–225. doi:10.1111/j.1469-8137.2006.01881.x
- Heraud, P., B. R. Wood, M. J. Tobin, J. Beardall, and D. McNaughton. 2005. Mapping of nutrient-induced biochemical changes in living algal cells using synchrotron infrared microspectroscopy. *FEMS Microbiol. Lett.* **249**: 219–225. doi:10.1016/j.femsle.2005.06.021
- Hirschmugl, C. J., Z. E. Bayarri, M. Bunta, J. B. Holt, and M. Giordano. 2006. Analysis of the nutritional status of algae by Fourier transform infrared chemical imaging. *Infrared Phys. Technol.* **49**: 57–63. doi:10.1016/j.infrared.2006.01.032
- Horton, R. B., E. Duranty, M. McConico, and F. Vogt. 2011. Fourier transform infrared (FT-IR) spectroscopy and improved principal component regression (PCR) for quantification of solid analytes in microalgae and bacteria *Appl. Spectrosc.* **65**: 442–453. doi:10.1366/10-06122
- Kansiz, M., P. Heraud, B. Wood, F. Burden, J. Beardall, and D. McNaughton. 1999. Fourier Transform Infrared microspectroscopy and chemometrics as a tool for the discrimination of cyanobacterial strains. *Phytochemistry* **52**: 407–417. doi:10.1016/S0031-9422(99)00212-5
- Mariey, L., J. Signolle, C. Amiel, and J. Travert. 2001. Discrimination, classification, identification of microorganisms using FTIR spectroscopy and chemometrics. *Vibrat. Spectrosc.* **26**: 151–159. doi:10.1016/S0924-2031(01)00113-8
- Moran, X. A. G., Á. Lopez-Urrutia, A. Calvo-Diaz, and W. K. W. Li. 2010. Increasing importance of small phytoplankton in a warmer ocean. *Global Change Biol.* **16**: 1137–1144. doi:10.1111/j.1365-2486.2009.01960.x
- Movasaghi, Z., S. Rehman, and D. ur Rehman. 2008. Fourier transform infrared (FTIR) spectroscopy of biological tissues. *Appl. Spectrosc. Rev.* **43**: 134–179. doi:10.1080/05704920701829043
- Murdock, J. N., W. K. Dodds, and D. L. Wetzel. 2008. Subcellular localized chemical imaging of benthic algal nutritional content via HgCdTe array FT-IR. *Vibrat. Spectrosc.* **48**: 179–188. doi:10.1016/j.vibspec.2007.12.011
- Murdock, J. N., and D. L. Wetzel. 2009. FT-IR Microspectroscopy enhances biological and ecological analysis of algae. *Appl. Spectrosc. Rev.* **44**: 335–361. doi:10.1080/05704920902907440
- Murdock, J. N., and D. L. Wetzel. 2012. Macromolecular response of individual algal cells to nutrient and atrazine mixtures within biofilms. *Microb. Ecol.* **63**: 761–772. doi:10.1007/s00248-011-9994-5
- Nasse, M. J., and others. 2011. High-resolution Fourier-transform infrared chemical imaging with multiple synchrotron beams. *Nat. Methods* **8**: 413–416. doi:10.1038/nmeth.1585
- Noguchi, T., and M. Sugiura. 2003. Analysis of flash-induced FTIR difference spectra of the S-state cycle in the photosynthetic water-oxidizing complex by uniform  $^{15}\text{N}$  and  $^{13}\text{C}$  isotope labeling. *Biochemistry.* **42**: 6035–6042. doi:10.1021/bi0341612

- Richardson, T. L., and G. A. Jackson. 2007. Small phytoplankton and carbon export from the surface ocean. *Science*. **315**: 838–840. doi:10.1126/science.1133471
- Sabine, C. L., and others. 2004. The oceanic sink for anthropogenic CO<sub>2</sub>. *Science* **305**: 367–371. doi:10.1126/science.1097403
- Sackett, O., and others. 2014. Taxon-specific responses of Southern Ocean diatoms to Fe enrichment revealed by synchrotron radiation FTIR microspectroscopy. *Biogeoscience* **11**: 5795–5808. doi:10.5194/bg-11-5795-2014
- Sanders, R. W., and K. G. Porter. 1988. Phagotrophic phytoflagellates, p. 167–192. *In* Anonymous advances in microbial ecology. Springer.
- Sayre, R. 2010. Microalgae: The potential for carbon capture. *Bioscience*. **60**: 722–727. doi:10.1525/bio.2010.60.9.9
- Sekkal, M., P. Legrand, J. P. Huvenne, and M. C. Verdus. 1993. The use of FTIR microspectrometry as a new tool for the identification insitu of polygalactanes in red seaweeds. *J. Mol. Struct.* **294**: 227–230. doi:10.1016/0022-2860(93)80356-Z
- Sigee, D. C., F. Bahrami, B. Estrada, R. E. Webster, and A. P. Dean. 2007. The influence of phosphorus availability on carbon allocation and P quota in *Scenedesmus subspicatus*: A synchrotron-based FTIR analysis. *Phycologia* **46**: 583–592. doi:10.2216/07-14.1
- Stehfest, K., J. Toepel, and C. Wilhelm. 2005. The application of micro-FTIR spectroscopy to analyze nutrient stress-related changes in biomass composition of phytoplankton algae. **43**: 717–726. doi:10.1016/j.plaphy.2005.07.001
- Stuart, B. 2005. Infrared spectroscopy. Wiley.
- Tortell, P. D., G. H. Rau, and F. M. Morel. 2000. Inorganic carbon acquisition in coastal Pacific phytoplankton communities. *Limnol. Oceanogr.* **45**: 1485–1500. doi:10.4319/lo.2000.45.7.1485
- Worley, B., S. Halouska, and R. Powers. 2013. Utilities for quantifying separation in PCA/PLS-DA scores plots. *Anal. Biochem.* **433**: 102–104. doi:10.1016/j.ab.2012.10.011
- Yamane, Y., T. Utsunomiya, M. Watanabe, and K. Sasaki. 2001. Biomass production in mixotrophic culture of *Euglena gracilis* under acidic condition and its growth energetics. *Biotechnol. Lett.* **23**: 1223–1228. doi:10.1023/A:1010573218863

### Acknowledgments

I thank Ruvini Omattage for laboratory assistance, and K. Henderson and N. Knorp provided comments that improved this manuscript. J. Rimoldi provided use of the benchtop FTIR microscope. I also thank L. Miller for facilitating the use of synchrotron infrared beamline U2B. The National Synchrotron Light Source of Brookhaven National Laboratory, Upton, NY, is operated as a user facility by the U.S. Department of Energy under contract no. DE-AC02-98CH10886. This work was funded by the U.S. Department of Agriculture, Agricultural Research Service.

Submitted 30 June 2015

Revised 9 October 2015

Accepted 17 October 2015

Associate editor: Claudia Benitez-Nelson